J. metamorphic Geol., 2002, **20,** 845–858

Fluid inclusions as microchemical systems: evidence and modelling of fluid–host interactions in plagioclase

B. KLEINEFELD[1] AND R. J. BAKKER[2]
[1]*FB 5, Faculty of Geosciences, University of Bremen, Postfach 330440, D-28334 Bremen, Germany (bkleinefeld@uni-bremen.de)*
[2]*Institute of Geosciences, Mineralogy & Petrology, University of Leoben, Peter-Tunner-Str. 5 -8700 Leoben, Austria*

ABSTRACT Dense, CO_2-rich fluid inclusions hosted by plagioclases, An_{45} to An_{54}, of the O.-v.-Gruber- Anorthosite body, central Dronning Maud Land, East Antarctica, contain varying amounts of small calcite, paragonite and pyrophyllite crystals detected by Raman microspectroscopy. These crystals are reaction products that have formed during cooling of the host and the original CO_2-rich H_2O-bearing enclosed fluid. Variable amounts of these reaction products illustrates that the reaction did not take place uniformly in all fluid inclusions, possibly due to differences in kinetics as caused by differences in shape and size, or due to compositional variation in the originally trapped fluid. The reaction albite + 2anorthite + $2H_2O$ + $2CO_2$ = pyrophyllite + paragonite + 2calcite was thermodynamically modelled with consideration of different original fluid compositions. Although free H_2O is not detectable in most fluid inclusions, the occurrence of OH-bearing sheet silicates indicates that the original fluid was not pure CO_2, but contained significant amounts of H_2O. Compared to an actual fluid inclusion it is obvious, that volume estimations of solid phases can be used as a starting point to reverse the retrograde reaction and recalculate the compositional and volumetrical properties of the original fluid. Isochores for an unmodified inclusion can thus be reconstructed, leading to a more realistic estimation of *P–T* conditions during earlier metamorphic stages or fluid capturing.

Key words: fluid inclusions; stepdaughters; back reactions; feldspar; anorthosite.

INTRODUCTION

The interpretation of many fluid inclusion studies is based on the assumption that the entrapped fluid has not changed its composition and density during the long exhumation history. Fluid inclusions, both primary and secondary, form during precipitation processes of a mineral host. At this stage, the enclosed fluid and its host crystal are not chemically reactive. However, at temperatures and pressures different from the formation conditions, the microsystem may become unstable and therefore react. Quartz, the most studied host mineral, is not chemically reactive with most of the enclosed fluids over a wide range of *P–T* conditions. The occurrence of chemical reactions between the entrapped fluid and a reactive mineral host (e.g. feldspar and pyroxene) has been reported so far by only a few workers.

Andersen *et al.* (1984) described inclusions in pyroxene from mantle xenoliths with a residual composition of nearly pure CO_2 and two secondary solids of carbonate and amphibole. It was suggested that both phases resulted from reaction between the pyroxene host and an original H_2O-CO_2-rich entrapped fluid. They used SEM and microprobe techniques to identify the varying entrapped minerals in fluid inclusions, and Raman microspectrometry for the analysis of fluid components. The density change of the remaining fluid was modelled against the volume change of the solid phase involved in the reaction. The reaction of melt inclusions with a garnet host was described by Schulze (1985). Included olivine is supposed to react with garnet to form spinel and pyroxene, which are later transformed into serpentine. Davis *et al.* (1990) reported the reaction of a salt-saturated aqueous solution in fluid inclusions with a halite host during a freezing-heating experiment. A rim presumably composed of hydrohalite formed just after the melting of ice. Heinrich & Gottschalk (1995) introduced the term 'back-reactions' for decarbonation reaction during retrogression in wollastonite-hosted fluid inclusions leading to the formation of quartz and calcite. On heating in the microstage, the progress of the prograde reaction is estimated visually and then thermodynamically modelled, using compositions and densities of similar but unmodified fluids entrapped in neighbouring quartz. Svensen *et al.* (1999, 2001) considered that some of the many entrapped crystals (e.g. calcite, quartz and K-feldspar) within fluid inclusions in omphacite and garnet may be reaction products of fluid and host ('stepdaughter crystals'), whereas the others were accidentally trapped during multiple re-opening or precipitated out of a supersaturated fluid.

Thermodynamic modelling of fluid-host reactions as applied to wollastonite by Heinrich & Gottschalk (1995) allows a more precise and realistic interpretation

of fluid inclusions analysed in metamorphic rocks. In this study we have combined the varying approaches of the previously described studies, including the exact analysis of reaction products as well as the thermodynamic evaluation of the stability field of phases involved and their proper mass balance. Plagioclase from the O.-v.-Gruber-Anorthosite complex, central Dronning Maud Land, East Antarctica, contains CO_2-rich fluid inclusions with several solid phases, which were identified as carbonates and sheet-silicates by Raman microspectrometry. The aim of this study is to prove that the enclosed solids formed by chemical reaction between the fluid and the host mineral.

GEOLOGICAL SETTING

Central Dronning Maud Land (cDML) is situated within the East Antarctic/African Orogen, the Late Neoproterozoic-Lower Palaeozoic collision zone between East and West-Gondwana (Jacobs *et al.*, 1998). One striking feature of this region is the occurrence of a massif-type anorthosite body that crops out over approximately 250 km^2 within the Otto-von-Gruber-Gebirge, East Antarctica (Fig. 1).

The volcanic and sedimentary basement rocks of cDML experienced an early Grenville-age metamorphic overprint at high- to medium-pressure granulite facies conditions (D1 and M1 according to Bauer *et al.*, 2003), that was associated with the syntectonic intrusion of granite sheets and plutons at *c.* 1085–1075 Ma (Jacobs *et al.*, 1998). Voluminous anorthositic magmas were emplaced at *c.* 600 Ma and the margins of the anorthosite body were strongly deformed at *c.* 580–550 Ma (Jacobs *et al.*, 1998). Deformation took place at medium-pressure granulite facies conditions of about 6.8 ± 0.5 kbar and 830 ± 20 °C and is interpreted as representing the collisional stage between East and West Gondwana, i.e. Pan-African I (Markl & Piazolo, 1998; D2 and M2 in Bauer *et al.*, 2003). During deformation the anorthosite body behaved like a large delta-clast that still exhibits undeformed magmatic textures in its central parts (Bauer *et al.*, 2003).

A subsequent tectono-metamorphic event (Pan-African II) started with the syntectonic intrusion of granitoids and gabbros at approximately 530 Ma and finally culminated in voluminous anorogenic charnockite and syenite magmatism at 510 Ma (Mikhalsky *et al.*, 1997; Jacobs *et al.*, 1998). Metamorphic conditions were at low–pressure granulite facies of 4–5 kbar and temperatures of about 640 ± 10 °C (Markl & Piazolo, 1998; D3/M3 in Bauer *et al.*, 2003). A poorly developed and yet undated retrogression at pressures of approximately 2–5 kbar and 480–580 °C postdates the voluminous intrusion of granitoids at 510 Ma (Markl & Piazolo, 1998; D4 in Bauer *et al.*, 2003).

Thermobarometric studies indicate a clockwise *P–T* path characterised by an isothermal decompression

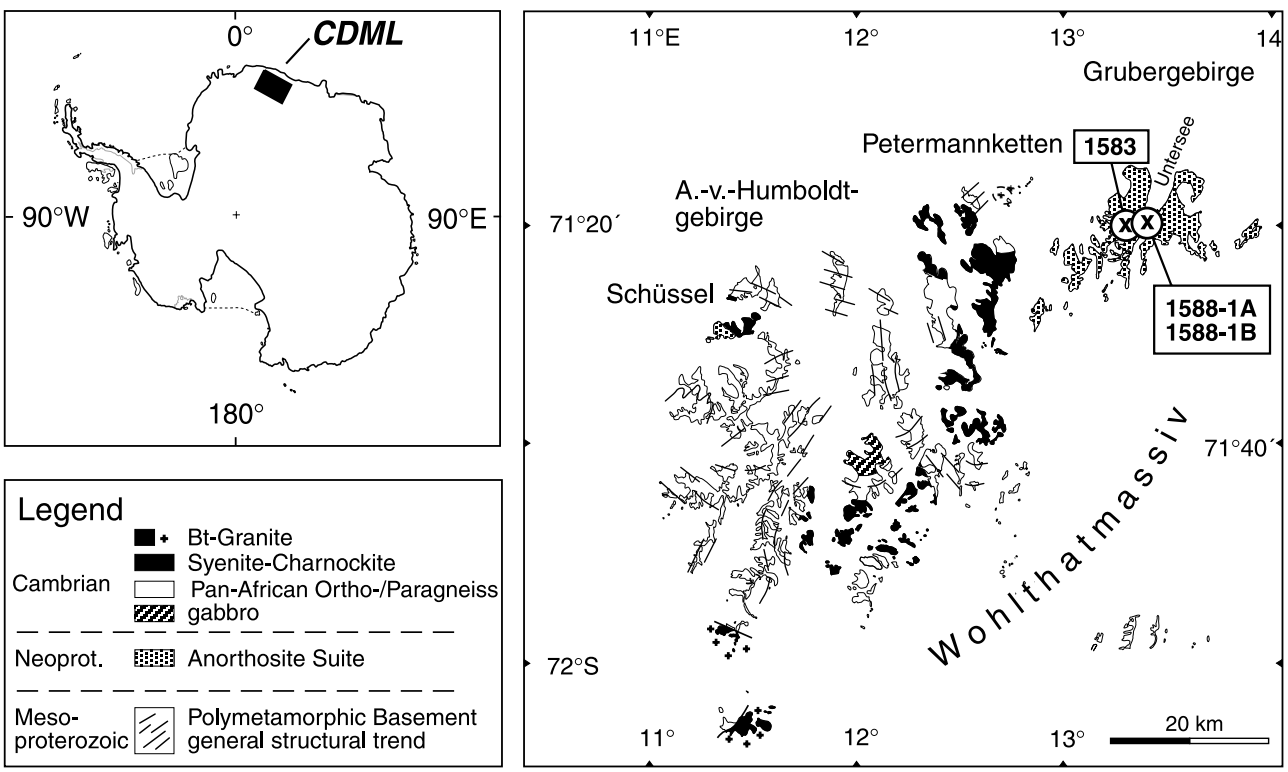

Fig. 1. Geological overview map of central Dronning Maud Land (CDML) and sample localities (modified after Jacobs *et al.*, 1998).

evolution for the early Pan-African I event, whereas the structures of the Pan-African II event are ascribed to a late-orogenic extensional collapse of the East Antarctic-African Orogen (Jacobs *et al.*, 2003).

ANALYTICAL METHODS

Thin- and thick-sections were made from selected samples, and investigated by optical petrography, electron microprobe analysis, microthermometry and Raman microspectrometry. Microthermometric measurements were carried out with a Linkam MDS 600 stage operating over a temperature range from −190 to 35 °C. Within these limits it was calibrated using synthetic fluid inclusions provided by Fluid Inc. at −56.6 and 0.0 °C, i.e. melting of pure CO_2 and pure H_2O, respectively. The analytical accuracy is ± 0.1 °C. The stage is mounted on an Olympus BX 60 microscope, modified and supplied by Fluid Inc. A Dilor LABRAM confocal-Raman spectrometer equipped with a frequency-doubled Nd-YAG laser (100 mW, 532.2 nm) with a LMPlanFI 100x/0.80 objective lens (Olympus) was used to identify fluid and solid phases in inclusions. Wavenumber measurements have an accuracy of 1.62 cm^{-1} at low Δv (Raman shift around 0 cm^{-1}) and 1.1 cm^{-1} at high Δv (around 3000 cm^{-1}). To analyse a homogeneous carbonic gas mixture by microspectrometry, samples were held at controlled temperatures of c. + 33 °C with a Linkam THMSG 600 heating-freezing stage. As the Raman signal for ice is more pronounced than for water, inclusions are analysed at −120 °C to verify the presence or absence of invisible small amounts of H_2O.

As the amount of N_2 detected by Raman microspectrometry does not exceed 2 mole%, fluid properties were calculated as being equivalent to pure CO_2. The error in molar volume estimation resulting from this assumption is by far smaller than liquid-vapour equilibrium calculations with published equations of state. Thus, molar volumes of these fluid inclusions are obtained from the homogenisation temperatures using the equation of Duschek *et al.* (1990) for pure CO_2 and isochore calculations are based on the equation of state of Span & Wagner (1996). Isochores for H_2O-CO_2 mixtures are calculated with the equation of state of Holloway, 1977, 1981). The fluid properties of homogeneous H_2O-CO_2-NaCl mixtures are calculated with the equation of state of Anderko & Pitzer (1993) and Duan *et al.* (1995). The salinity of rare H_2O-CO_2-NaCl fluid inclusions hosted by quartz is calculated using the program *Q2* from the software package CLATHRATES (Bakker, 1997). All other fluid properties were computed with the software package FLUIDS (Bakker, in press).

An ARL-SEMQ 30 microprobe equipped with four wavelength-dispersive spectrometers (WDS) with TAP, LiF and PET diffraction crystals, and a LINK AN 10/25S energy-dispersive spectrometer (EDS) was used to measure plagioclase compositions. Beam conditions were 20 kV and 15 nA. A plagioclase standard from the Leoben University was used for calibration. The Bastin correction was applied to the obtained data.

PETROGRAPHY AND MICROPROBE ANALYSIS

The light-grey anorthosite rocks are fine to coarse-grained equigranular and bimodal inequigranular with plagioclase megacrysts up to 1.5 cm in size. The major constituent is plagioclase (*c.* 90 vol.%) of An_{45} to An_{54} (Fig. 2, and ortho- and clinopyroxene occur in varying minor amounts. Quartz, biotite, hornblende, chlorite, opaque (oxides and sulphides), sheet-silicates, K-feldspar (microcline) and carbonates form accessories, some of which are related to the metamorphic overprint.

Large subhedral to euhedral grains of plagioclase are slightly flattened and may show lattice-preferred orientation. Antiperthitic unmixing is often observed in larger grains. Twinning on albite- and pericline law planes is common (Fig. 3a). Bent deformation lamellae and undulose extinction in addition to subgrain formation and subgrain rotation and bulging of grain boundaries give evidence of intracrystalline deformation and recovery, probably related to the Pan-African I metamorphic event. Aggregates of small, dynamically recrystallized grains surround the larger feldspar clasts (Fig. 3b) and thus form 'core-and-mantle' structures (as described by Passchier & Trouw, 1996). Within these fine-grained areas a polygonal fabric with relatively straight grain boundaries has developed. Rare intercrystalline microfractures are either open or filled with sheet silicates and/or calcite. Some plagioclase crystals show strong alteration to sericite and calcite, whereas ortho- and clinopyroxene may be altered to hornblende and biotite along small intracrystalline fractures and grain boundaries.

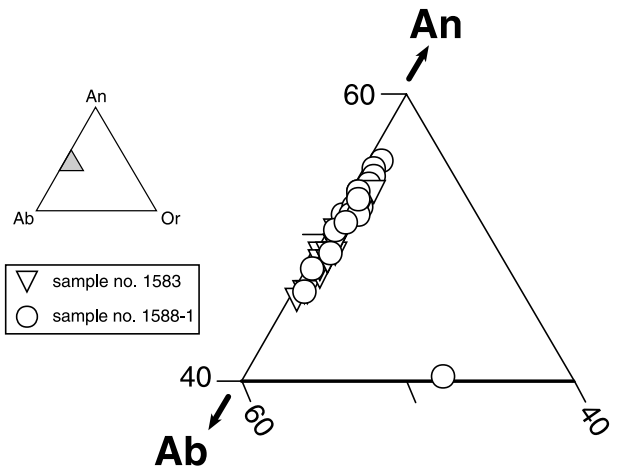

Fig. 2. Feldspar compositions obtained from electron microprobe analysis plotted in the ternary Or–Ab–An diagram.

RESULTS OF FLUID INCLUSION STUDIES

Fluid inclusion petrography

One single type of fluid inclusions hosted by plagioclase was identified within all anorthosite samples. Inclusions have an average length of 7–15 μm (longest dimension), but sizes down to 2.5 μm and up to 65 μm were also observed (Table 1). Inclusion shapes vary from roundish or oval to negative-crystal shapes (Fig. 4a). At room temperature, they contain a single liquid-like carbonic phase and occasionally several birefringent solid phases (Fig. 4b). The solid/fluid ratio varies significantly among adjacent inclusions. Fluid inclusions are arranged as intracrystalline clusters (Fig. 4c) and trails (Fig. 4d), thus giving evidence of pseudosecondary origin, as they do not crosscut grain boundaries. Rarely, the accumulated appearance

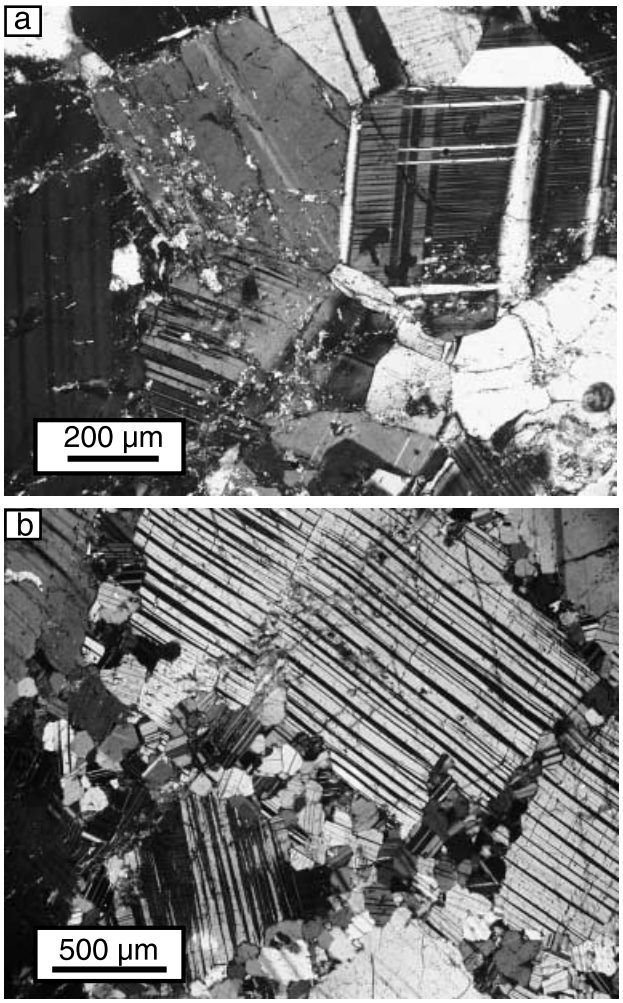

Fig. 3. Microphotographs of albite and pericline-twins in plagioclase of sample 1583 (a) and 'core-and-mantle' structures of sample 1588–1 (b).

of fluid inclusions at the centre of large feldspar crystals, best visible in sections perpendicular to the c-axis, give evidence of relictic magmatic growth zonation in plagioclase. In some crystals, alignment of fluid inclusions along single twin lamellae was observed.

Aside from this dominant type of fluid inclusions hosted by plagioclase, accessory xenomorphic quartz also contains some inclusions. These are approximately 3–10 μm in size, rounded to negative crystal shape. In general they comprise an aqueous liquid and a carbonic vapour phase, the latter occupying from 30 vol% up to an apparent total fill (Fig. 4e). Decrepitation clusters occur around some inclusions that contain only a carbonic vapour phase (Fig. 4f).

Composition of plagioclase adjacent to fluid inclusions

Electron microprobe analysis reveals that there is no evidence for significant chemical gradients in feldspar around single fluid inclusions (Fig. 5). Potassium variation is close to nil whereas Al, Ca and Na ranges of *c.* 2 wt%. No systematic relationship between composition and distance from inclusion could be detected. The average composition of plagioclase around this particular inclusion is $An_{46}Ab_{53}Or_1$ to $An_{53}Ab_{46}Or_1$ (see appendix, Table A1).

Microthermometry and Raman microspectrometry of the enclosed fluid

Upon cooling from room temperature, the inclusions first nucleate a gas bubble around 0 °C before supercooling leads to the formation of a solid phase around −90 °C. Upon heating, melting of the solid phase occurs within a narrow temperature range of −57.8 to −56.8 °C (Fig. 6 & Table 1). CO_2 was confirmed by Raman microspectrometry as being the major gaseous component within all fluid inclusions hosted by plagioclase. The lowering of the final melting temperature of pure CO_2 is caused by the addition of small amounts of N_2 (maximally 2 mol%) whereas CH_4 and H_2O were never detected. All fluid inclusions homogenise into the liquid phase over a broad temperature interval of −1.8 to 27.3, with the majority homogenising between 14 and 20 °C (Fig. 6 and Table 1). There is no systematic relationship between Th and Tm.

Quartz-hosted fluid inclusions reveal a similar CO_2-melting point of −57.7 °C and additional clathrate melting was observed around 7.9 °C. Homogenisation of CO_2 occurred at 18.7 °C into the liquid phase. The calculated salinity obtained from the clathrate melting temperature is equivalent to 4.2 wt% NaCl. In addition to CO_2, small amounts of N_2 were identified with Raman microspectrometry. The presence of H_2O was even confirmed in those inclusions that did not show a visible aqueous rim (e.g. Fig. 4f). Entrapped minerals were not detected within these inclusions.

Raman microspectrometry of enclosed solids

Because of their high refractive index compared to the surrounding plagioclase, carbonate crystals entrapped in fluid inclusions can easily be identified by optical microscopy (Fig. 4b). Raman spectrometry is able to detect even slight variations in carbonate composition (Bischoff *et al.*, 1985), and a shift of Raman peaks from 284, 714 and 1087 cm^{-1} to 283, 711 and 1085 cm^{-1} shows, that the enclosed minerals are Mg-enriched (< 10 mol% $MgCO_3$) or pure calcite (Table 1), respectively.

Sheet silicates are often located at the inclusion walls or at carbonate crystal faces and may easily be overlooked in small or dark fluid inclusions. The Raman peaks of muscovite and paragonite are similar, not further differentiated in this study and therefore more generally referred to as dioctahedral mica. Nevertheless, paragonite is thought to make up most of the enclosed mica, as K is only a minor component of the feldspar host. The Raman spectra for dioctahedral

Table 1. Microthermometrical data, length (in μm) and molar volume (in $cm^3\ mol^{-1}$) of carbonic (car) fluid inclusions. Melting (T_m) and homogenisation temperatures (T_h) are given in °C. Homogenisation is always into the liquid phase. The solid phases calcite (cal), Mg-calcite (mg-cal), dioctaedral mica (dm) and pyrophyllite (prl) were identified with Raman spectroscopy. Numbers in brackets indicate the volume percentage of the specific solid phase. The occurrence of at least one solid phase that was not further identified is indicated by '+'.

Inclusion no.	Length (μm)	Solid Phases	T_m (car) °C	T_h (car) °C	V_M ($cm^3\ mol^{-1}$)
1583-1-01	14.5	+	−57.1	14.3	53.20
1583-1-02	7.5	+	−57.2	12.2	52.13
1583-1-03	9.0	+	−57.3	6.6	49.71
1583-1-04	4.5	+	−57.3	10.2	51.20
1583-1-05	5.0	+	−57.3	5.8	49.41
1583-1-06	13.0	mg-cal	−57.1	7.5	50.06
1583-1-07	9.0	+	−57.3	27.3	65.64
1583-1-08	11.0	mg-cal	−57.3	10.6	51.38
1583-1-09	30.0	mg-cal	−57.0	22.8	59.39
1583-1-10	9.0		−57.0	7.9	50.22
1583-1-11	9.0		−57.0	6.3	49.60
1583-1-12	9.0	mg-cal	−57.0	1.1	47.80
1583-1-13	7.5	+	−57.2	15.6	53.93
1583-1-14	14.0	cal (25), dm (12)	−56.7	7.1	49.91
1583-1-15	11.0	+	−56.8	10.8	51.47
1583-1-16	5.0	+	−56.8	4.6	48.97
1583-1-17	10.0		−56.8	17.5	55.11
1583-1-18	14.0	cal	−57.2	16.5	54.47
1583-1-19	11.0	+	−56.9	18.5	55.79
1583-1-20	7.0	mg-cal	−56.9	19.2	56.29
1583-1-21	65.0	mg-cal (11), dm (3)	−56.8	18.5	55.79
1583-3-03	15.0	mg-cal (5), dm-prl (6)	−57.1	8.7	50.55
1583-3-04	27.0	mg-cal (34), dm-prl (9)	−57.1	20.9	57.64
1583-3-05	7.0	mg-cal (6), dm-prl (6)	−57.1	11.4	51.74
1583-3-06	30.0	mg-cal (34), dm-prl (4)	−57.0	17.0	54.79
1583-3-07	17.0	mg-cal (34)	−57.2	−1.8	46.92
1583-3-08	8.0	mg-cal (5), dm-prl (7)	−57.3	1.0	47.77
1588–1 A-1–01	13.0		−56.8	19.4	56.44
1588–1 A-1–02	9.5	+	−56.9	16.8	54.66
1588–1 A-1–03	9.5		−56.8	19.9	56.82
1588–1 A-1–04	11.0		−56.8	19.9	56.82
1588–1 A-1–05	8.0		−57.0	14.5	53.31
1588–1 A-1–06	5.5		−57.0	17.3	54.98
1588–1 A-1–07	5.5	+	−56.9	17.1	54.85
1588–1 A-1–08	2.5		−57.1	17.4	55.04
1588–1 A-1–09	7.0		−57.1	18.0	55.44
1588–1 A-1–10	2.5	+	−57.0	17.2	54.91
1588–1 A-1–11	3.5		−57.1	18.9	56.07
1588–1 A-1–12	6.0		−57.1	16.6	54.54
1588–1 A-2–13	22.0	cal, mg-cal (2)	−57.5	15.7	53.99
1588–1 A-2–14	8.5	+	−57.5	14.4	53.26
1588–1 A-2–15	15.0	mg-cal	−57.5	18.0	55.44
1588–1 A-2–16	18.5	cal, prl	−57.5	17.4	55.04
1588–1 A-2–17	6.5	mg-cal	−57.5	18.4	55.72
1588–1 A-2–18	10.0	mg-cal	−57.5	17.4	55.04
1588–1 A-2–19	8.5	mg-cal	−57.4	18.2	55.58
1588–1 A-2–20	8.5	cal	−57.5	16.2	54.29
1588–1B-3–22	30.0	mg-cal (8), prl (4)	−57.3	14.1	53.1
1588–1B-3–23	7.0		−57.3	15.9	54.11
1588–1B-3–24	10.0		−57.3	17.2	54.91
1588–1B-3–25	15.5		−57.3	12.5	52.27
1588–1B-3–26	14.5	mg-cal	−57.3	20.6	57.38
1588–1B-3–27	14.5		−57.6	18.1	55.51
1588–1B-3–28	16.5		−57.8	17.2	54.91
1588–1B-3–29	15.0		−57.6	15.7	53.99

mica and pyrophyllite are similar up to a Raman shift of about 1200 cm^{-1} (Fig. 7). Both have an intense peak at 264 cm^{-1}, whereas the second peak is slightly higher for pyrophyllite (708 cm^{-1}) than for dioctahedral mica (702 cm^{-1}). Most diagnostic peaks appear at higher wavenumbers, between 3600 and 3700 cm^{-1}, where different types of O-H bonds in the mineral structure are detectable. The sharp peak for pyrophyllite at 3674 cm^{-1} is clearly distinct from the broad peak for dioctahedral mica at 3626 cm^{-1} (Fig. 7b). Both minerals were identified within fluid inclusions where they appear as individual crystals or intergrown aggregates (Fig. 7, Table 1).

DISCUSSION

The microchemical reaction

Fluid-inclusion studies have proved that feldspar-hosted inclusions from the O.-v.-Gruber-Anorthosite

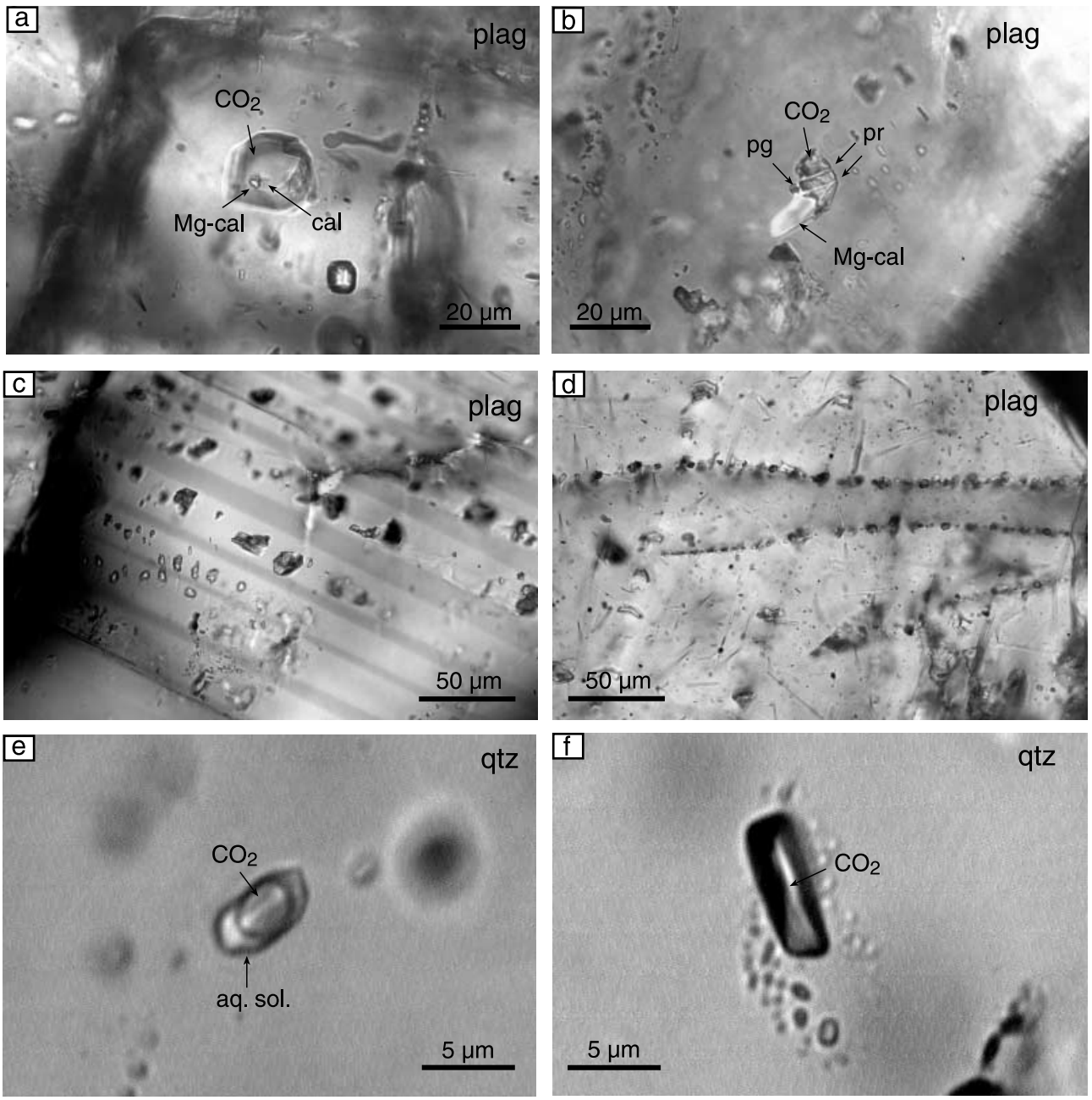

Fig. 4. Microphotographs of CO_2-rich fluid inclusions hosted by plagioclase: (a) negative-crystal shaped inclusions containing carbonate crystals; (b) containing various birefringent crystals; (c) cluster between albite twins; (d) pseudosecondary trails; (e) two phase inclusion in quartz, containing a CO_2-rich bubble and a H_2O-rich rim; (f) decrepitation cluster around an apparently carbonic-rich fluid inclusion in quartz.

body commonly contain a dense CO_2-rich gas mixture together with different volume fractions of solids, i.e. calcite, pyrophyllite and a dioctahedral mica. The frequent occurrence of this characteristic feature throughout the samples rules out the possibility of accidental trapping (capturing). Additionally, the lack of H_2O, and the varying amounts of solids present suggest that it is very unlikely that the solids formed as daughter crystals out of a supersaturated fluid/melt. We therefore assume that the solids have developed as products of reaction (1) or (2).

$$[NaAlSi_3O_8 + 2CaAl_2Si_2O_8]^{plag} + [2H_2O + 2CO_2]^{fluid} \leftrightarrow [Al_2Si_4O_{10}(OH)_2]^{prl} + [NaAl_2Si_3AlO_{10}(OH)_2]^{pg} + [2CaCO_3]^{cal} \quad (1)$$

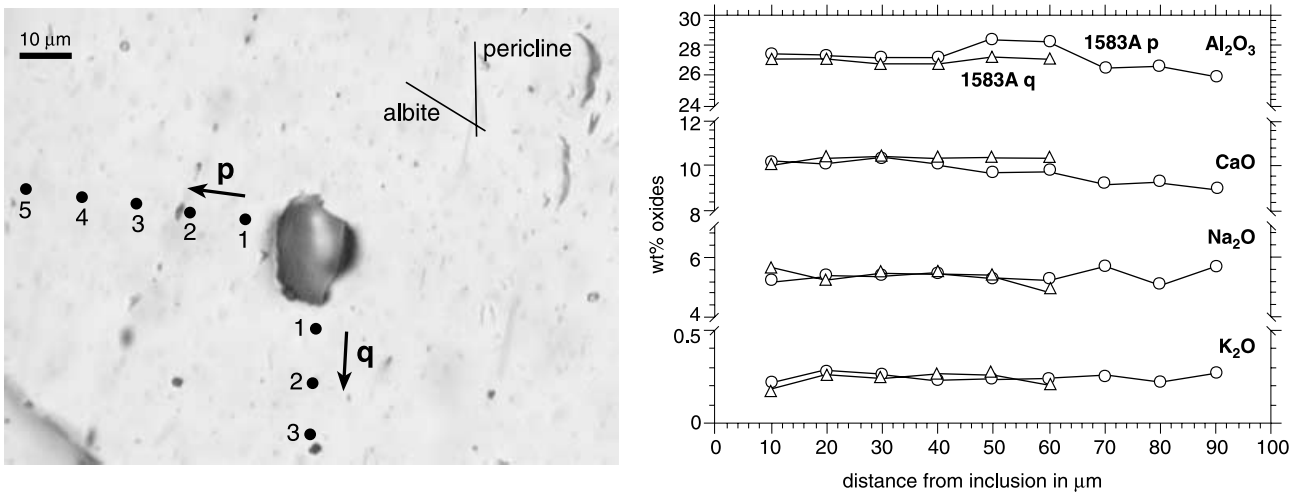

Fig. 5. Al_2O_3, CaO, Na_2O and K_2O concentrations (in wt%) along two profiles around a fluid inclusions. 0 μm marks the inclusion wall. Profiles 'p' and 'q' are perpendicular to each other. The orientation of albite and pericline twins is schematically indicated by thin lines.

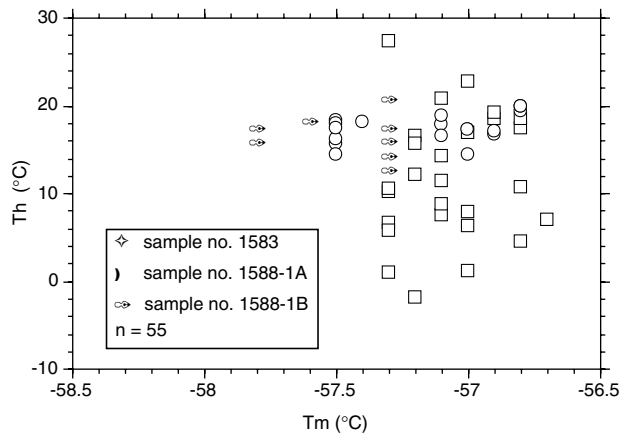

Fig. 6. Th-Tm plot of CO_2-dominated fluid inclusions hosted by plagioclase. Freezing-point depression is caused by N_2-contents of up to 2 mol%; all inclusions homogenise into the liquid phase.

$$[KAlSi_3O_8 + 2CaAl_2Si_2O_8]^{plag} + [2H_2O + 2CO_2]^{fluid} \leftrightarrow [Al_2Si_4O_{10}(OH)_2]^{prl} + [KAl_2Si_3AlO_{10}(OH)_2]^{pg} + [2CaCO_3]^{cal} \quad (2)$$

As the plagioclases is low in K (Fig. 2), it is more likely that reaction (1) predominated during the interaction between the host mineral and the fluid. The thermodynamic data of the individual components involved in the reaction were taken into account to determine the *P–T* stability field of products and reactants (Appendix B). The proposed reaction within fluid inclusions takes place if the rock *P–T* conditions move into the stability field of the products. The position of the reaction curves in a *P–T* diagram is dependent on the initial fluid composition (Fig. 8). A mixture of 50:50 mol mixture of H_2O and CO_2 defines the maximum

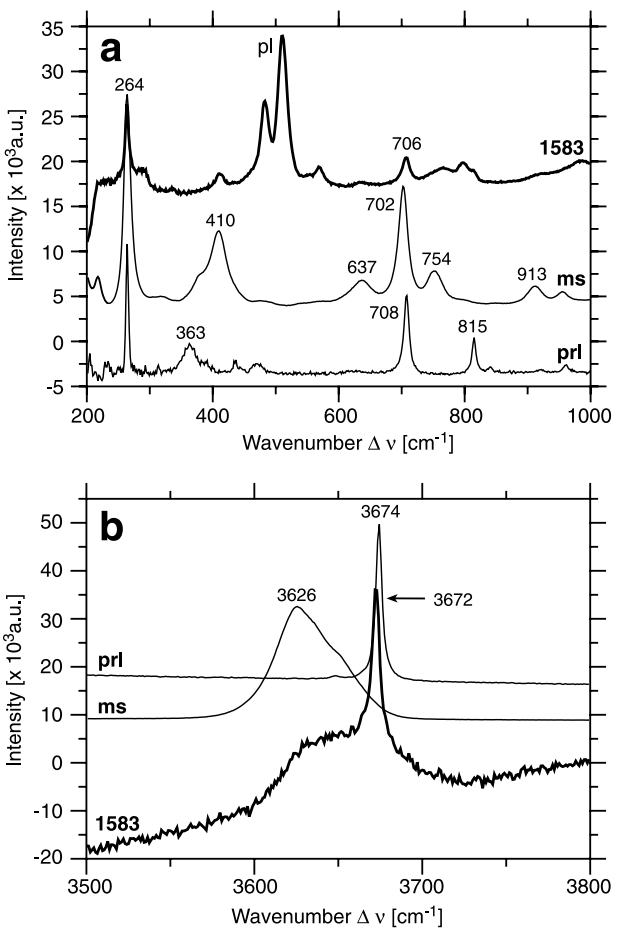

Fig. 7. Raman spectrum of sheet silicates from sample 1583 in different ranges of the Raman shift Δv: (a) 200–1000 cm^{-1}; (b) 3500–3800 cm^{-1}. Standard spectra of muscovite (ms) (substitutional for the dioctahedral micas) and pyrophyllite (prl) are indicated as a reference. pl = background peak of plagioclase host.

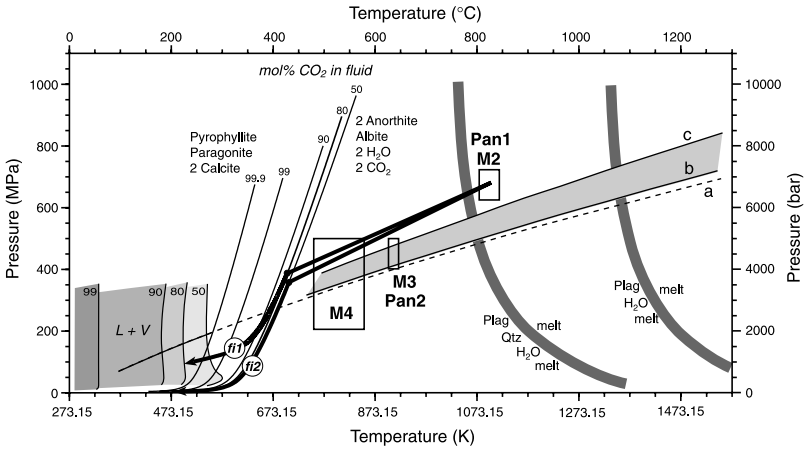

Fig. 8. Temperature–pressure diagram with reaction curves calculated for fluid compositions of 50, 80, 90, 99 and 99.9 mol% CO_2. The immiscibility field of the corresponding H_2O-CO_2-fluid mixture after Tödheide & Franck (1963) is illustrated at relatively low temperatures (L + V). M2, M3 and M4 indicate the metamorphic conditions as described in the text. Pan1 and Pan2 illustrate the *P–T* conditions of the Pan-African event, collosional stage I and II, respectively. Isochores for hypothetical inclusions *fi1* and *fi2* that formed at M2, and the path of reaction progress according to the change in fluid composition during interaction between fluid and host-mineral are shown by thick black lines. The isochore for inclusion 1583-3-08, presently containing pure CO_2 is indicated by dashed curve a. Also shown are corrected isochores according to our model (curve b for 97.2 mol% CO_2 and 45.55 cm^3 $mole^{-1}$, and curve c for 93.6 mol% CO_2 and 42.66 cm^3 mol^{-1}). The shaded area between curve b and c represents the uncertainty in the reconstruction of this specific inclusion. The approximate liquidi of the systems An-Ab-H_2O and An-Ab-Qtz-H_2O, according to Johannes (1978, 1989) are illustrated at relatively high temperatures (thick grey lines), indicating possible formation conditions of fluid inclusions in crystallizing plagioclase.

reaction temperature in the amphibolite facies, whereas the reaction temperatures are lower for all other mixtures. The immiscibility fields of H_2O–CO_2 mixtures, according to Tödheide & Franck (1963), do not interfere with the reaction for any fluid composition (Fig. 8 and Appendix B). The immiscibility fields of CO_2-rich fluids in the H_2O-CO_2-NaCl system also do not have interference with the reaction (Appendix B). Reaction (2) occurs at temperatures well below those given for metamorphic conditions in cDML by Markl & Piazolo (1998) and therefore it must have taken place at a late stage of crustal evolution (post M4). The presence of carbonate and sheet silicates in most fluid inclusions indicates that the reaction has indeed proceeded. The occurrence of sheet silicates requires the presence of H_2O within the inclusions before the reaction took place. The quartz hosted fluid inclusions have a comparable distribution and contain similar gaseous components. Therefore it is suggested that both, quartz- and plagioclase-hosted inclusions, have a common origin. As quartz is nonreactive and these inclusions still contain small amounts of H_2O (Fig. 4e), the original fluid composition in plagioclase is considered to have had a water component, too. We propose that a CO_2-H_2O-rich fluid was originally trapped as fluid inclusions, and that this reacted with its plagioclase host, leading to complete consumption of the subordinate aqueous fluid-component, the formation of a residual carbonic liquid and the crystallization of carbonates and sheet silicates (Fig. 9a,c). The actual fluid preserved in quartz must not unequivocally reflect the original fluid properties as quartz-hosted inclusions might have changed by mechanical and diffusional processes since their formation. These reequilibration processes may result in decrepitation and preferential water loss as has been proved by experimental work (e.g. Sterner & Bodnar, 1989; Bakker & Jansen, 1991). Decripitation clusters and a variation in the enclosed amount of water have been observed in fluid inclusions in quartz (Fig. 4f).

The lack of any carbonates or sheet silicates in some of the plagioclase-hosted CO_2-rich inclusions and the variable volume fraction of the reaction products can be explained by a variation in the original fluid composition. Furthermore, the same reequilibration processes that have previously been described for quartz may have effected the plagioclase. Microstructures preserved in plagioclase crystals (Fig. 3) imply that these processes have occurred. Kinetics may be responsible for the noncompletion of reactions which again results in a diversity of inclusion contents.

The model

Considering a fluid inclusion as a closed system, a quantitative model was established to describe volumetric and compositional changes caused by reaction (1). Two hypothetical fluid inclusions of the H_2O-CO_2 binary (*fi1* and *fi2* in Fig. 8) are assumed to have been trapped at M2 metamorphic conditions, with initial fluid compositions of 80 mol% CO_2 and 50 mol% CO_2, respectively (molar volumes are 38.93 cm^3 mol^{-1} and 33.32 cm^3 mol^{-1}, respectively). With favourable kinetics, both inclusions start to react when the system

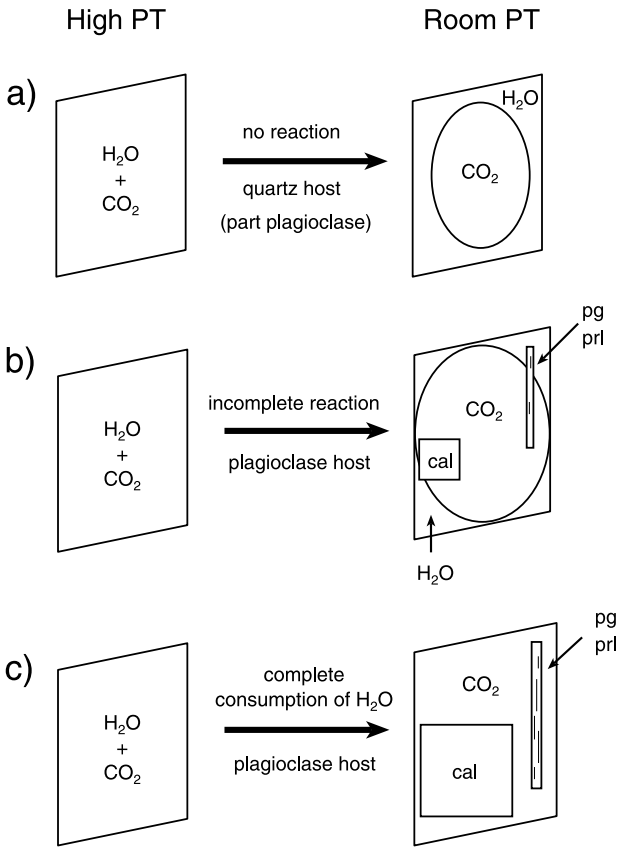

Fig. 9. Schematic reaction progress in a closed fluid-inclusion system with an original homogeneous H_2O-CO_2 fluid not containing any solid phases at high *P–T*. (a) No reaction for inclusions in quartz and part of the plagioclase. (b) After occurrence of part of the reaction in only plagioclase. (c). After complete consumption of H_2O and formation of larger calcite, paragonite and pyrophyllite volume fractions.

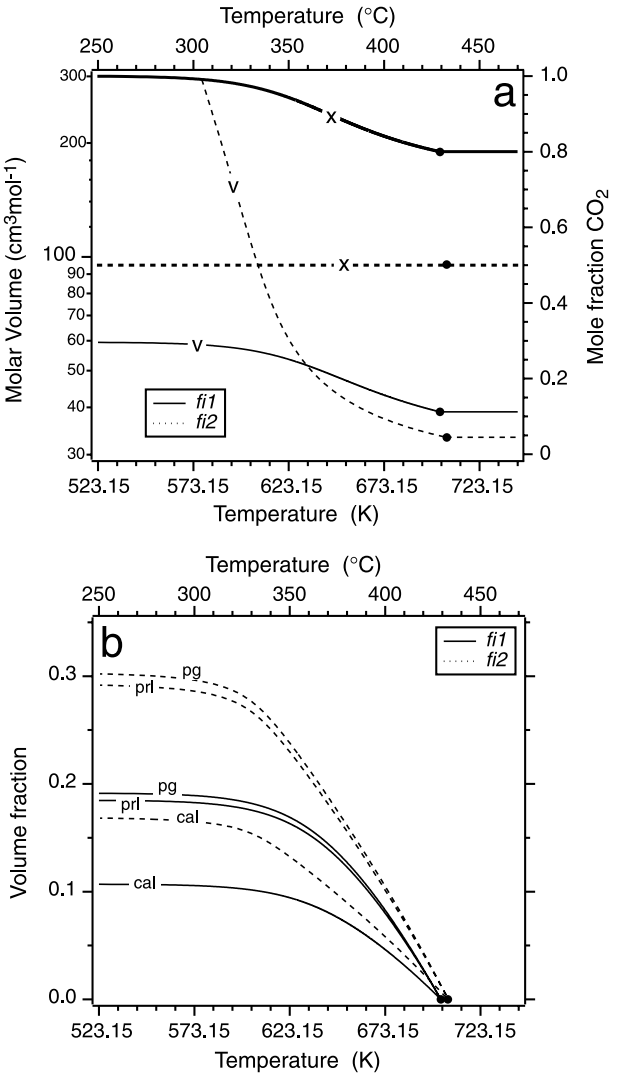

Fig. 10. Influence of the retrograde reaction on hypothetical fluid inclusions *fi1* (initially 80 mol% CO_2) and *fi2* (initially 50 mol% CO_2). The solid dots indicate the starting point of the reactions. (a) The change in molar volume and fluid composition caused by cooling after the reaction curves are reached at about 450 °C. (b) Amount of solid reaction products forming during cooling.

reaches the corresponding reaction curves at about 450 °C. With progressive reaction, these inclusions develop in different ways. The molar volume of *fi1* reaches a maximum value of about 59.5 cm^3 mol^{-1} at lower temperatures, which is a nearly pure CO_2 liquid-like fluid, whereas *fi2* continuously increases its molar volume up to a vapour-like fluid (Fig. 10a). The fluid composition in *fi2* does not change. The f*i1* volume percentages will be 10.7 calcite, 18.5 pyrophyllite and 19.1 paragonite after the reaction is nearly complete at lower temperatures (Fig. 10b). The volume percentages of solid reaction products in *fi2* are higher, i.e. 16.9 calcite, 29.3 pyrophyllite and 30.3 paragonite. These amounts may not be reached if the reaction ceases when the kinetics becomes unfavourable at lower temperatures. Vice versa, the evaluation of the amount of reaction products allows the recalculation of the composition and molar volume of the initial fluid.

Using a natural example, fluid inclusion *1583-3-08* (Table 1) presently contains a dense pure CO_2 liquid, *c*. 5 vol% calcite and *c*. 7 vol% of paragonite and pyrophyllite as visually estimated, corresponding to 1.355 mmole and 0.54 mmole, respectively, in a hypothetical fluid inclusion of 1 cm^3 total volume. At 1.0 °C, its CO_2 content homogenises to the liquid phase, which corresponds to a molar volume of 47.77 cm^3 mol^{-1}, or a total mount of 18.42 mmole CO_2 in 1 cm^3 total volume. In order to model the density change of the fluid phase, the equation from Andersen *et al.* (1984) has been slightly modified to take into consideration the temperature and pressure effect on molar volumes of the solid phases (from Berman, 1988). To reverse reaction (1) and recalculate the original fluid composition and density, there are two possible formulations with which to start. First, the estimated amount of bound-H_2O in sheet silicates

(7 vol.%) is used as fixed parameter. In this case, 0.54 mmole of H_2O and CO_2 is calculated to have been consumed in the reaction with the formation of 0.54 mmole calcite and sheet silicates. Therefore, the original inclusion contained 0.54 mmole H_2O and 18.96 mmole CO_2 (i.e. 2.8 mol% H_2O and 97.2 mol% CO_2) resulting in a molar volume of this fluid is 45.55 cm^3 mol^{-1}. However, the actual inclusion contains a total amount of 1.355 mmol calcite, meaning that there is 0.815 mmole calcite in excess (i.e. 3 vol.%). This suggests that part of the observed carbonate may have been accidentally trapped during initial inclusion formation, or perhaps the measurement of 7 vol.% of sheet silicates is in error.

In the second approach, calculations were performed assuming that calcite will be consumed completely during the inversion of reaction (1). In this case, more sheet silicates than the amount estimated by optical observations must be taken into account for the reaction to proceed, i.e. 0.6775 mmole paragonite and 0.6775 mmole pyrophyllite. Sheet silicates often form as thin layers on inclusion walls and on carbonates, and might therefore be easily overlooked during optical microscopy. As illustrated in Fig. 10(b), the calculated amount of sheet silicates produced by the progress of reaction (1) is always higher than the amount of carbonates. This situation is in agreement with the observed room-temperature volume ratios of carbonates to sheet silicates. The initial fluid derived in this way contains 6.4 mol% H_2O and 93.6 mol% CO_2, with a molar volume of 42.66 cm^3 mol^{-1}.

After reaction (1) has completed, the maximum amount of calcite within fluid inclusions that formed at M2 conditions is about 16.9 vol% (see Fig. 10b). However, several observed inclusions are estimated to contain up to 34 vol% calcite, e.g. inclusion no. *1583-3-07* (Table 1). Taking into account difficulties in volume-fraction estimations of sheet silicates, this inclusion would have originally contained 28.6 mol% H_2O and 71.4 mol% CO_2, with an extremely high molar volume of 24.99 cm^3 mol^{-1}. These reconstructed fluid properties are unrealistic within the known framework of geological events for the samples. It is therefore likely that part of the calcite was indeed accidentally trapped. As the plagioclase also contains small solid inclusions of pure carbonate, it is possible that the fluid inclusions are pinned to its grain-boundaries.

Although the model results diverge slightly from the estimated volume percentages of the solid phases at room temperature, they accord with respect to the characteristics of the original fluid inclusion: it must have contained some water, it was of higher density, and the formation of solid phases via reaction with the inclusion walls reduced the total free fluid volume by about 1–2.5 vol%. Thus, cooling of the host rock from M2 metamorphic conditions caused a simultaneous decrease in density and total volume, while at the same time various solids formed upon complete consumption of the aqueous component.

Reconstructed isochores

Recalculated isochores of the assumed original fluid compositions and densities, e.g. lines b and c in Fig. 8, are shifted towards higher pressures than those estimated for the present state of inclusions at room temperature (line a in Fig. 8). Considering the fluid inclusions formed at an early stage of the rock development, they may have originated immediately after crystallization of a plagioclase-rich melt of intermediate composition. The pseudo-secondary character of most inclusion trails confirms this early formation at granulite facies conditions. As the presence of a host crystal is a necessity for the formation of fluid inclusions, the liquidus of the plagioclase system theoretically defines the maximum formation conditions. However, it is more likely that inclusions formed shortly after completion of the crystallization of the magma, i.e. at solidus conditions. The original magma systems must have contained certain amounts of dissolved CO_2 and H_2O. The system albite-anorthite-H_2O (Johannes, 1978) has a liquidus at about 1100 °C at 500 MPa water pressure (Fig. 8). The addition of small amounts of quartz to this system can drastically lower the liquidus temperature to about 800 °C at 500 MPa and to about 900 °C at 200 MPa (Johannes, 1978, 1989). Data for a CO_2 bearing system are not available, but it will transpose both liquidus and solidus to higher pressures at a selected temperature.

The intersection of the corrected isochores from fluid inclusion 1583-3-08 (Fig. 8) with the albite-anorthite-H_2O liquidus are at about 1080 °C and 650–730 MPa. However, much higher pressures will be obtained from those inclusions that contain a higher volume percentage of reaction products. This may give important constrains on possible *P–T* conditions for the emplacement of the anorthositic magmas between M1 and M2 metamorphism (Bauer *et al.*, 2003), which could not be estimated by other means.

CONCLUSIONS

The combined use of laser-Raman spectrometry and microthermometry has characterised a complete microchemical reaction system hosted by plagioclase. Submicroscopic phases (fluid and solid) covering inclusion walls, and optically visible solids were identified as carbonates, muscovite/paragonite and pyrophyllite, together with a nearly pure, dense CO_2 fluid phase. These solids are assumed to have developed as products of reaction between the fluid and its host. The OH-bearing sheet silicates are interpreted as proof of an aqueous component within the originally entrapped fluid. The amount of H_2O initially available in the trapped fluid is considered to control the extent of the retrograde reaction. With all involved phases identified, the reaction was thermodynamically modelled and the *P–T* stability conditions of products and reactants were determined, as a function of the fluid

compositions. Quantitative analysis on the basis of volume estimates of the solid reaction-products found in plagioclase-hosted fluid inclusions were used to recalculate the composition and molar volume of the original fluid. The deviation in the ratio of carbonate to sheet silicates formed within the hypothetical and the real inclusions lies within the uncertainty limits of the method. Thin layers of sheet silicates can be easily overlooked during microscopy and it is possible that part of the carbonate was accidentally trapped at the time of inclusion formation. The results have shown that detailed fluid inclusion studies combined with thermodynamic modelling can be used to trace back and evaluate the changes that a fluid inclusion has undergone since its formation. Thus, valuable petrogenetic information can be derived and used for more precise estimation of *P–T* conditions during earlier metamorphic stages or fluid entrapment.

ACKNOWLEDGEMENTS

This work is part of the PhD thesis of B. Kleinefeld funded by the FNK, University of Bremen, Germany, reference number 05/134/7. M. Olesch is thanked for providing the rock samples and field data collected during the GeoMaud Expedition 95/96 granted by the German Research Foundation (OL 25/9). The technical support of V. Kolb, H. Mühlhans and P. Witte is greatly appreciated. L. Diamond kindly made constructive remarks on the manuscript and improvements on the English. B.K. is grateful for the use of technical facilities of the Institute of Geosciences, Mineralogy & Petrology, University of Leoben, Austria. T. Andersen and W. Heinrich are thanked for constructive reviewing.

REFERENCES

Anderko, A. & Pitzer, K. J., 1993. Equation of state representation of phase equilibria and volume tric properties of the system NaCl-H_2O above 573 K. *Geochimica et Cosmochimica Acta*, **57,** 1657–1680.

Andersen, T., O'Reilly, S. Y. & Griffin, W. L., 1984. The trapped fluid phase in upper mantle xenoliths from Victoria, Australia; implications for mantle metasomatism. *Contributions to Mineralogy and Petrology*, **88,** 72–85.

Bakker, R. J., 1997. Clathrates: Computer Programs to calculate fluid inclusion V–X properties using clathrate melting temperatures. *Computers and Geosciences*, **23,** 1–18.

Bakker, R. J., in press. Package *FLUIDS* 1. Computer programs for analysis of fluid inclusion data and for modelling bulk fluid properties. *Chemical Geology*, in press.

Bakker, R. J. & Jansen, J. H. B., 1991. Experimental post-entrapment water loss from synthetic CO_2-H_2O inclusions in natural quartz. *Geochimica et Cosmochimica Acta*, **55,** 2215–2230.

Bauer, W., Jacobs, J. & Paech, H.-J., 2003. Structural evolution of the Crystalline Basement of central Dronning Maud Land. *East Antarctica. Geologisches Jahrbuch*, *B96*, in press.

Berman, R. G., 1988. Internally-consitent thermodynamic data for minerals in the system Na_2O-K_2O-CaO-MgO-FeO-Fe_2O_3-Al_2O_3-SiO_2-TiO_2-H_2O-CO_2. *Journal of Petrology*, **29,** 445–522.

Bischoff, W. D., Sharma, S. K. & Mackenzie, F. T., 1985. carbonate disorder in synthetic and biogenetic magnesian calcites: a Raman spectral study. *American Mineralogist*, **70,** 581–589.

Davis, D. W., Lowenstein, T. K. & Spencer, R. J., 1990. Melting behavior of fluid inclusions in laboratory grown halite crystals in the systems NaCl-H_2O, NaCl-KCl-H_2O, NaCl-$MgCl_2$-H_2O and NaCl-$CaCl_2$-H_2O. *Geochimica et Cosmochimica Acta*, **54,** 591–601.

Duan, Z., Møller, N. & Weare, J. H., 1995. Equation of state for the NaCl-H_2O-CO_2 system: Prediction of phase equilibria and volume tric properties. *Geochimica et Cosmochimica Acta*, **59,** 2869–2882.

Duschek, W., Kleinrahm, R. & Wagner, W., 1990. Measurement and correlation of the (pressure, density, temperature) relation of carbon dioxide. II. Saturated-liquid and saturated-vapour density and the vapour pressure along the entire coexistence curve. *Journal of Chemical Thermodynamics*, **22,** 841–864.

Elkins, L. T. & Grove, T. L., 1990. Ternary feldspar experiments and thermodynamic models. *American Mineralogist*, **75,** 544–559.

Flowers, G. C., 1979. Correction of Holloway's (1977) adaption of the modified Redlich-Kwong equation of state for calculation of fugacities of molecular species in supercritical fluids of geological interest. *Contributions to Mineralogy and Petrology*, **69,** 315–318.

Gehrig, M., 1980. Phasengleichgewichte und PVT-daten ternärer Mischungen aus Wasser, Kohlendioxid und Natriumchlorid bis 3 kbar und 550 °C. *PhD Thesis*, *University Karlsruhe, Hochschulverlag, Freiberg Germany*.

Heinrich, W. & Gottschalk, M., 1995. Metamorphic reactions between fluid inclusions and mineral hosts; I, Progress of the reaction calcite + quartz = wollastonite + CO_2 in natural wollastonite-hosted fluid inclusions. *Contributions to Mineralogy and Petrology*, **122,** 51–61.

Holloway, J. R., 1977. Fugacity and activity of molecular Species in supercritical fluids. In: *Thermodynamics in geology. NATO ASI. Series D*. (ed. Fraser, D. G.), pp. 161–182. Reidel, Dordrecht.

Holloway, J. R., 1981. Compositions and Volumes of supercritical fluids in the earth's crust. In: *Short Course in Fluid Inclusions: Application to Petrology* (eds Hollister, L. S. & Crawford, M. L.), pp. 13–38, Mineralogical Association of Canada, Calgary.

Jacobs, J., Fanning, C. M., Henjes, K. F., Olesch, M. & Paech, H. J., 1998. Continuation of the Mozambique Belt into East Antarctica; Grenville-age metamorphism and polyphase Pan-African high-grade events in central Dronning Maud Land. *Journal of Geology*, **106,** 385–406.

Jacobs, J., Klemd, R., Fanning, C. M., Bauer, W. & Colombo, F., 2003. Extensional collapse of the Late Neoproterozoic/Early Palaeozoic East African/Antarctic Orogen in central Dronning Maud Land. In: Proterozoic East Gondwana: Supercontinent Assembly and Break-up, (eds Yoshida, M., Windley, B. F. & Dasgupta, S.). *Journal of the Geological Society of London*. Special Publications.

Johannes, W., 1978. Melting of plagioclase in the system Ab-An-H_2O and Qz-Ab-An-H_2O at P_{H_2O} = 5 kbars, an equilibrium problem. *Contributions to Mineralogy and Petrology*, **66,** 295–303.

Johannes, W., 1989. Melting of plagioclase-quartz assemblages at 2 kbar water pressure. *Contributions to Mineralogy and Petrology*, **103,** 270–276.

Krüger, Y. & Diamond, L. W., 2001. P-V-T-X properties of two H_2O-CO_2-NaCl mixtures up to 850 °C and 500 MPa: a synthetic fluid inclusion study. XVI. ECROFI. *Faculdade de Ciências Do Porto, Departamiento de Geologia, Memória*, **7,** 241–244.

Markl, G. & Piazolo, S., 1998. Halogen-bearing minerals in syenites and high-grade marbles of Dronning Maud Land, Antarctica; monitors of fluid compositional changes during late-magmatic rock–rock interaction processes. *Contributions to Mineralogy and Petrology*, **132,** 246–268.

Mikhalsky, E. V., Beliatsky, B. V., Savva, E. V., Wetzel, H. U., Federov, L. V., Weiser, T. & Hahne, K., 1997. Reconnaissance Geochronologic Data on Polymetamorphic and Igneous rocks of the Humboldt Mountains, central Queen Maud Land, East Antarctica. In: *The Antarctic Region: Geological Evolution and Processes* (ed. Ricci, C. A.), pp. 45–53. Terra Antarctica Publication, Siena, Italy.

Passchier, C. W. & Trouw, R. A. J., 1996. *Microtectonics*. Springer-Verlag, Berlin.

Schulze, D. J., 1985. Evidence for primary kimberlite liquids in megacrysts from kimberlites in Kentucky, USA. *Journal of Geology*, **93,** 75–80.

Span, R. & Wagner, W., 1996. A new equation of state for carbon dioxide covering the fluid region from the triple point temperature to 1100 K at pressures up to 800 MPa. *Journal of Physical Chemistry Reference Data*, **25,** 1509–1596.

Sterner, S. M. & Bodnar, R. J., 1989. Synthetic fluid inclusion; VII, Re-equilibration of fluid inclusions in quartz during laboratory simulated metamorphic burial and uplift. *Journal of Metamorphic Geology*, **7,** 243–260.

Svensen, H., Jamtveit, B., Banks, D. A. & Austrheim, H., 2001. Halogen contents of eclogite facies fluid inclusions and minerals; Caledonides, western Norway. *Journal of Metamorphic Geology*, **19,** 165–178.

Svensen, H., Jamtveit, B., Yardley, B., Engvik, A. K., Austrheim, H. & Broman, C., 1999. Lead and bromine enrichment in eclogite-facies fluids: Extreme fractionation during lower crustal hydration. *Geology*, **27,** 467–470.

Tödheide, K. & Franck, E. U., 1963. Das Zweiphasengebiet und die kritische Kurve im System Kohlendioxid-Wasser bis zu Drucken von 3500 bar. *Zeitschrift Physikalische Chemie. Neue Folge*, **37,** 387–401.

Received 25 January 2002; revision accepted 2 July 2002.

APPENDIX A

Table A1. Microprobe analysis of plagioclase around the fluid inclusion illustrated in Fig. 5.

Sample	Gruber Fjella Anorthosite – sample 1583, plagioclase analysis														
Analysis	p.1	p.2	p.3	p.4	p.5	p.6	p.7	p.8	p.9	q.1	q.2	q.3	q.4	q.5	q.6
SiO_2	54.57	55.05	55.15	56.03	54.73	54.50	56.34	55.66	56.36	56.19	55.52	56.01	56.31	53.97	54.97
TiO_2	0.00	0.00	0.00	0.00	0.00	0.00	0.00	0.00	0.00	0.00	0.00	0.00	0.00	0.00	0.00
Al_2O_3	27.40	27.23	27.11	27.14	28.27	28.23	26.48	26.58	25.89	27.02	27.01	26.63	26.67	27.20	27.04
Cr_2O_3	0.00	0.00	0.00	0.00	0.00	0.00	0.00	0.00	0.00	0.00	0.00	0.00	0.00	0.00	0.00
FeO	0.10	0.17	0.17	0.10	0.07	0.15	0.10	0.12	0.07	0.05	0.17	0.05	0.07	0.17	0.10
Fe_2O_3	0.00	0.00	0.00	0.00	0.00	0.00	0.00	0.00	0.00	0.00	0.00	0.00	0.00	0.00	0.00
MgO	0.05	0.05	0.05	0.00	0.00	0.00	0.10	0.00	0.05	0.00	0.05	0.05	0.00	0.05	0.10
MnO	0.00	0.00	0.00	0.00	0.00	0.00	0.00	0.00	0.00	0.00	0.00	0.00	0.00	0.00	0.00
CaO	10.13	10.01	10.24	10.05	9.63	9.69	9.19	9.22	8.92	9.96	10.30	10.31	10.15	10.30	10.28
Na_2O	5.18	5.37	5.37	5.45	5.26	5.26	5.70	5.08	5.70	5.62	5.19	5.45	5.36	5.37	4.92
K_2O	0.21	0.27	0.25	0.22	0.23	0.23	0.26	0.22	0.27	0.17	0.25	0.23	0.25	0.24	0.21
Total	97.64	98.15	98.34	98.99	98.19	98.06	98.17	96.88	97.26	99.01	98.49	98.73	98.81	97.30	97.62
Si:	2.51	2.52	2.52	2.54	2.50	2.50	2.57	2.57	2.59	2.55	2.53	2.55	2.56	2.50	2.53
$Al^{(IV)}$:	0.00	0.00	0.00	0.00	0.00	0.00	0.00	0.00	0.00	0.00	0.00	0.00	0.00	0.00	0.00
Al:	1.49	1.47	1.46	1.45	1.52	1.52	1.42	1.45	1.40	1.44	1.45	1.43	1.43	1.49	1.47
Ti:	0.00	0.00	0.00	0.00	0.00	0.00	0.00	0.00	0.00	0.00	0.00	0.00	0.00	0.00	0.00
Cr:	0.00	0.00	0.00	0.00	0.00	0.00	0.00	0.00	0.00	0.00	0.00	0.00	0.00	0.00	0.00
Fe^{2+}:	0.00	0.01	0.01	0.00	0.00	0.01	0.00	0.00	0.00	0.00	0.01	0.00	0.00	0.01	0.00
Fe^{3+}:	0.00	0.00	0.00	0.00	0.00	0.00	0.00	0.00	0.00	0.00	0.00	0.00	0.00	0.00	0.00
Mg:	0.00	0.00	0.00	0.00	0.00	0.00	0.01	0.00	0.00	0.00	0.00	0.00	0.00	0.00	0.01
Mn:	0.00	0.00	0.00	0.00	0.00	0.00	0.00	0.00	0.00	0.00	0.00	0.00	0.00	0.00	0.00
Ca:	0.50	0.49	0.50	0.49	0.47	0.48	0.45	0.46	0.44	0.48	0.50	0.50	0.49	0.51	0.51
Na:	0.46	0.48	0.48	0.48	0.47	0.47	0.50	0.45	0.51	0.49	0.46	0.48	0.47	0.48	0.44
K:	0.01	0.02	0.01	0.01	0.01	0.01	0.02	0.01	0.02	0.01	0.01	0.01	0.01	0.01	0.01
Ab:	0.51	0.50	0.51	0.50	0.50	0.50	0.46	0.49	0.46	0.49	0.52	0.50	0.50	0.51	0.53
An:	0.47	0.49	0.49	0.50	0.49	0.49	0.52	0.49	0.53	0.50	0.47	0.48	0.48	0.48	0.46
Or:	0.01	0.02	0.02	0.01	0.01	0.01	0.02	0.01	0.02	0.01	0.02	0.01	0.02	0.01	0.01

APPENDIX B

Thermodynamics of Reaction

The coefficients in the formula for heat capacity and standard state properties of the minerals and gases involved in reaction 1 and 2 are taken from Berman (1988). The temperature and pressure dependency of molar volumes of minerals is also taken from Berman (1988). The Gibbs free energy calculation (B1) was used to determine the reaction in *p-T-V-x* space.

$$\Delta_R G = \sum_i v_i G_i = 0 \qquad \text{(Bla)}$$

$$\Delta_R G = G_{prl} + G_{pg} + 2G_{cc} - G_{ab} - G_{an} - 2G_{H_2O} - 2G_{CO_2} = 0 \qquad \text{(B1b)}$$

where v and G are the stoichiometric coefficient and the molar Gibbs free energy of the indicated phase, respectively. For each phase the change of Gibbs free energy with temperature, pressure and composition is expressed according to equation (B2).

$$dG = \left(\frac{\partial G}{\partial T}\right)_{P,n_i} dT + \left(\frac{\partial G}{\partial P}\right)_{T,n_i} dP + \sum_i \left(\frac{\partial G}{\partial n_i}\right)_{T,P,n_j} dn_i \qquad \text{(B2a)}$$

$$\left(\frac{\partial G}{\partial n_i}\right)_{T,P,n_j} = \mu_i \tag{B2b}$$

where T, P, and n are temperature, pressure and the amount of component i given in moles, respectively. μ_i is the chemical potential of component i. The reaction (1) involves a fluid mixture and a plagioclase mixture, whereas the reaction products pyrophyllite, paragonite and calcite are pure phases. Although, paragonite may include a calcium component and calcite may include a sodium component, the mass balance easily indicates that both margarite and sodium carbonate can not be obtained from the specific reactants in reaction (1), which is confirmed by Raman microspectrometry. The chemical potential of a component i in a mixture is calculated according to equation (B3).

$$\mu_i(T,P,x) = \mu_i^{pure}(T,P) + RT\ln(a_i) \tag{B3}$$

where x and a are the mole fraction and the activity of component i, respectively. This equation is also valid for pure phases, where the activity equals unity. The standard state condition for the fluid mixture is the thermodynamic properties of the pure components at the given temperature and 0.1 MPa, whereas properties of the pure components at the given temperature and pressure is the standard condition for the plagioclase. The chemical potential at standard conditions is obtained from the integration of the temperature and pressure dependent parameters in equation (B2a) (eq.B4).

$$\int_{T_0}^{T}\left(\frac{\partial G}{\partial T}\right)_{P_{0,n_i}} dT = \int_{T_0}^{T}(Cp)_{P_{0,n_i}} dT - S^0\cdot(T-T_0) - T\cdot\int_{T_0}^{T}\left(\frac{Cp}{T}\right)_{P_{0,n_i}} dT \tag{B4a}$$

$$\int_{P_0}^{P}\left(\frac{\partial G}{\partial P}\right)_{T,n_i} dP = \int_{P_0}^{P}(V)_{T,n_i} dP \tag{B4b}$$

where S^0 is the standard state entropy, Cp is the heat capacity at constant pressure, V is the molar volume, and T_0 and P_0 are the standard conditions, respectively.

The activity of fluid components is defined by the fugacities (f) of H_2O and CO_2 (eq.B5).

$$a_i = \frac{f_i(T,P)}{f_i^{pure}(T,P)} \tag{B5}$$

where i is either H_2O or CO_2. The fugacity of H_2O and CO_2 in gas mixtures was calculated with the modified Redlich-Kwong equation of state according to Holloway (1977, 1981) and Flowers (1979). This equation is the most accurate available thermodynamic model representing experimental fugacities of CO_2-H_2O fluids within the temperature and pressure limits of the reaction. The fugacity of fluid components in the ternary H_2O-CO_2-NaCl system are calculated with the equation of state from Anderko & Pitzer (1993) and Duan *et al.* (1995). The boundaries of the immiscibility field of CO_2-rich fluid mixtures are highly inaccurately estimated by this equation. Therefore, it is only applied to homogeneous mixtures.

The activities of albite and anorthite in the plagioclase are obtained from a nonideal mixing model for ternary feldspar according to Elkins & Grove (1990). This model is an empirical fit to experimental data on the feldspar compositions at temperatures between 600 and 900 °C, and at pure H_2O pressures between 100 MPa and 300 MPa. Although reaction (1) occurs at temperatures well below this fit, it is assumed that the estimated ternary Margules expression is also valid at lower temperatures.

The effect of several mixing models on the fluid and the plagioclase of reaction (1) is illustrated in Fig. B1. For any pressure, the maximum reaction temperature is defined at a fluid composition of approximately 50 mol% CO_2 and 50 mol% H_2O. The ideal mixing model for plagioclase causes a decrease of about 10 °C of the reaction temperature for any fluid composition compared to a model with unmixed plagioclase (Fig. B1a). The nonideal mixing model of plagioclase according to Elkins & Grove (1990) puts the reaction curve about 5 ° C higher than the ideal mixing model. Addition of small amounts of NaCl to the fluid mixture has a minor effect on the reaction temperature (Fig. B1b). In H_2O-rich fluids the reaction temperature is decreased by 0.2 and 0.5 °C for a 5 wt% and a 10 wt% NaCl solution, respectively. Additional NaCl in CO_2-rich fluids is a negligible factor. At higher pressures (Fig. B1c), the reaction curve is asymmetrical in a T-x diagram due to differences in the activities of H_2O and CO_2.

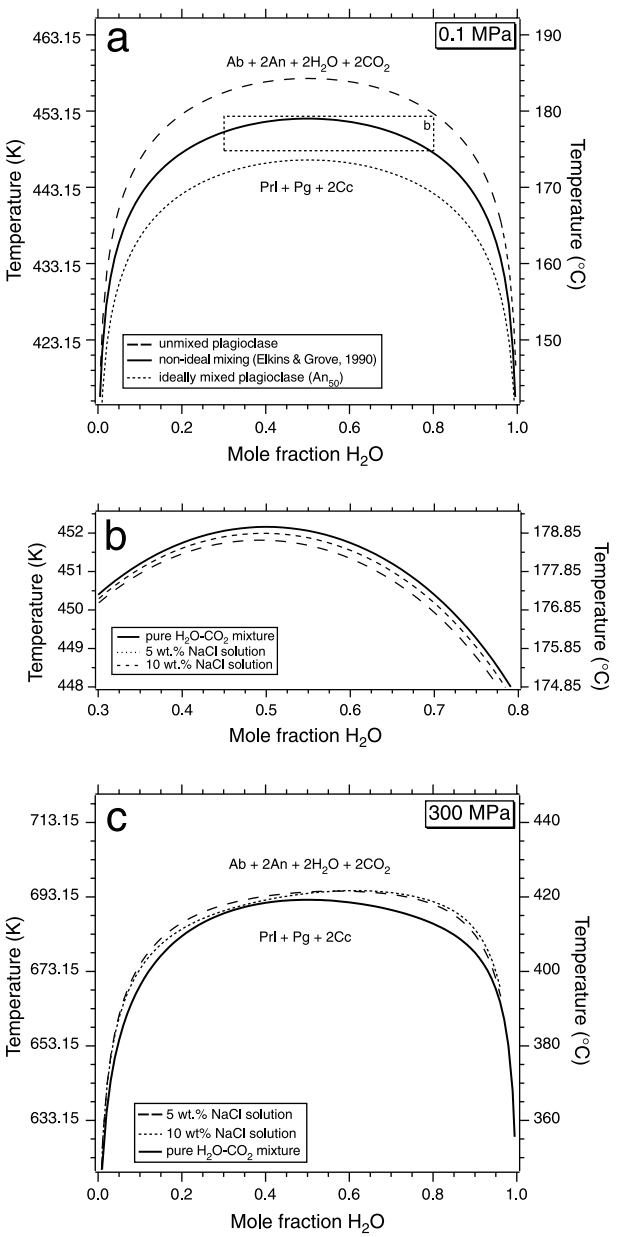

Fig. B1. Fluid composition (CO_2-H_2O) – temperature diagrams with reaction (1) according to different mixing models for the plagioclase at 0.1 MPa (a), the influence of 5 and 10 wt% NaCl solution at 0.1 MPa (b), and the reaction curve at 300 MPa with 5 and 10 wt% NaCl solution (c). The salinity is expressed relative to the amount of H_2O.

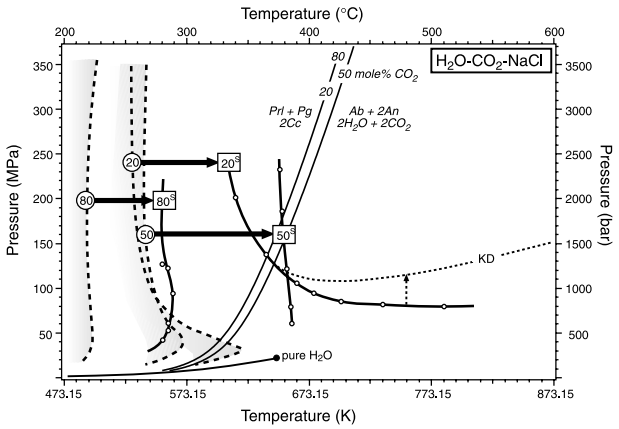

Fig. B2. Temperature – pressure diagram with the solvi of H_2O-CO_2 fluid mixtures (dashed curves) and the solvi of H_2O-CO_2 fluid mixtures with 6 wt% NaCl (solid curves). The numbers 80, 50, and 20 denote the mole percentage of CO_2. The superscript S. indicates the addition of 6 wt% NaCl to the corresponding fluid. The open circles are experimental data from Gehrig (1980). KD marks the corrected solvus of a 21.01-mol% CO_2, 77.47 mol% H_2O and 1.52 mol% NaCl fluid mixture (i.e. 6 wt% NaCl) according to Krüger & Diamond (2001). The reaction is illustrated for a 20, 50 and 80 mol% CO_2 fluid mixture.

The immiscibility field of H_2O-CO_2 mixtures is elevated to higher pressures and temperatures if certain amounts of NaCl are added to the system (Fig. B2). Experimental data from Tödheide & Franck (1963) and Gehrig (1980) illustrate, that the addition of 6 wt% NaCl to a fluid mixture of 50 mol% H_2O and 50 mol% CO_2 raises its solvus about 100 °C at variable pressures. A H_2O-rich fluid mixture has a large expansion of its immiscibility field to low pressures and higher temperatures (see also Krüger & Diamond, 2001), whereas the effect of the addition of NaCl diminishes with higher CO_2 contents. The reaction (1) between the entrapped fluids and the plagioclase appears to proceed mainly outside the immiscibility fields of salt-free systems. In a 6 wt.% NaCl solution, only H_2O-rich fluids, i.e. > 50 mol% H_2O, interfere with the reaction at about 380 °C, whereas CO_2-rich fluids remain homogeneous at reaction conditions. Within fluid inclusions in quartz salinities of < 6 wt% NaCl have been measured. Therefore, it can be concluded that there is no interference between the reaction and the immiscibility field at any conditions.